

# Towards Connectivity-Aware Pulmonary Airway Segmentation

Minghui Zhang and Yun Gu, *Member, IEEE*

**Abstract**— **Detailed pulmonary airway segmentation is a clinically important task for endobronchial intervention and treatment of peripheral pulmonary lesions. Convolutional Neural Networks (CNNs) are promising for automated analysis of medical imaging, which however performs poorly on airway segmentation. Specifically, breakage of small bronchi distals cannot be effectively eliminated in the prediction results of CNNs, which is detrimental to use as a reference for bronchoscopic-assisted surgery. In this paper, we proposed a connectivity-aware segmentation framework to improve the performance of airway segmentation. A Connectivity-Aware Surrogate (CAS) module is first proposed to balance the training progress within-class distribution. Furthermore, a Local-Sensitive Distance (LSD) module is designed to identify the breakage and minimize the variation of the distance map between the prediction and ground-truth. The proposed method is validated with the publically available reference airway segmentation datasets. The detected rate of branch and length on public EXACT'09 and BAS datasets are 82.1%/79.6% and 96.5%/91.5% respectively, demonstrating the effectiveness of the method in terms of improving the connectedness of the segmentation performance.**

**Index Terms**— **Pulmonary Airway Segmentation, Breakage and Refinement, Surrogate Loss**

## I. INTRODUCTION

ACCURATE airway segmentation is a prerequisite for both pre-operative planning and intra-operative navigation in endobronchial interventions. Due to the fine-grained pulmonary airway structure, manual annotation is time-consuming, error-prone, and highly relies on the expertise of clinicians. To alleviate such burdens and expedite the explorations of airways, automatic airway segmentation algorithms have been continuously explored. Thus far, public airway datasets with annotation (EXACT'09 [1], BAS [2]) are widely used to develop automatic airway extraction algorithms [2]–[7]. The performance of the airway extraction algorithms can be evaluated from two aspects, including overlap-wise accuracy and connectivity measurements. For overlap-wise accuracy measurements, the Dice Similarity Coefficient (DSC) metric is commonly used to measure the segmentation accuracy. DSC reflects the shape and dimension of the airways, and

The manuscript is received at 2022. This work was partly supported by National Key R&D Program of China (2019YFB1311503), Shanghai Sailing Program (20YF1420800), NSFC (62003208).

Minghui Zhang (minghuihang@sjtu.edu.cn), Yun Gu (geron762@sjtu.edu.cn) are with Institute of Image Processing and Pattern Recognition, Shanghai Jiao Tong University, 200240, Shanghai, CHINA.

these quantitative measurements are beneficial to the diagnosis of pulmonary diseases. Connectivity measurements, including the tree length detected rate (TD, %) and branch detected rate (BD, %), are used to measure the completeness and continuity of the predictions. Compared with other medical image segmentation tasks, airway segmentation task requires more attentions on connectivity. According to previous works [1], [7], [8], only the largest connected component of the airway result is useful to the bronchoscopic-assisted surgery. Under such circumstance, the connectivity is more critical than the overlap-wise accuracy. Unlike the general segmentation tasks which focus more on overlap-wise accuracy, the connectivity measurements are also important for airway segmentation as it reflects the intrinsic structure of the airway tree, which is particularly relevant for intra-operative navigation under physiological motion including respiration. In practice, ensuring connectivity is challenging as it is difficult to be achieved by only using the overlap-wise loss functions, e.g., Dice loss. Previous work [7] claimed that this can be attributed to the severe within-class distribution imbalance, as the trachea and principal bronchi dominate most of the voxels while the lobar bronchi and distal segmental bronchi only occupy a small proportion. Consequently, as shown in Fig.1(a) as an example, the baseline method trained with dice loss function generates a skew likelihood map that peripheral airways share a lower confidence probability than that of the principal bronchi.

A simple method to improve the local connectivity is to increase the recall of the foreground. However, even if the recall is higher, the overlap-wise loss functions are imperceptive to small breakages of the airway structures. To visualize this effect, we present the distance transformation map of the prediction in Fig.1(b) where voxel intensities illustrate the distance to the nearest boundary. It can be observed that the breakage merely induces marginal voxel-level errors while the connectivity is significantly changed. Hence, single supervision from the overlap-wise loss functions cannot guarantee promising connectedness.

To resolve the aforementioned issues, we propose a connectivity-aware model to facilitate the performance of airway segmentation. A Connectivity-Aware Surrogate Loss (CAS) is first proposed to balance the within-class distribution of airways. As observed by Qin *et al.* [8], the prediction binarized by a smaller threshold can boost a significant improvement of the TD/BD, while the DSC drops dramatically. As the threshold is relaxed, the recall metric of the foreground class will increase, and therefore the breakage problem is

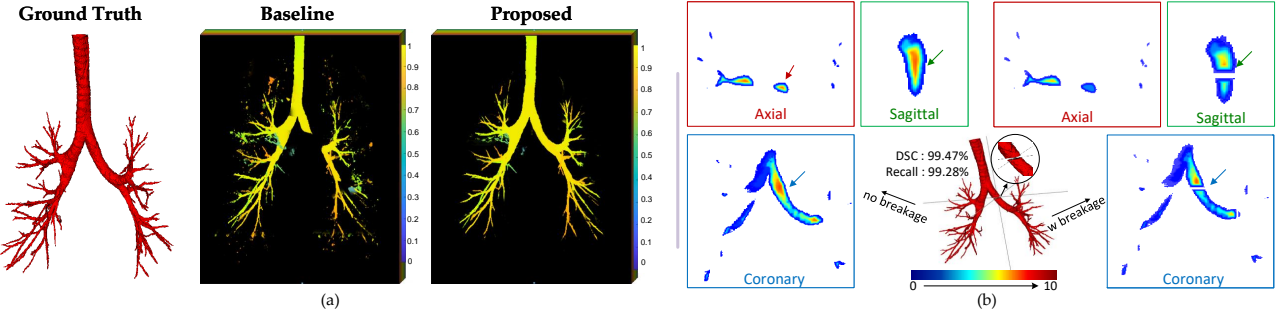


**Fig. 1.** Illustrations of discontinuous problems in airway segmentation: (a) Maximum intensity projection of the probability maps obtained from different methods. (b) Comparison between the distance transform map of the binary result with or without the breakage. In (a), the baseline generates a skewed likelihood map that peripheral airways share lower confidence probability than that of the principal bronchi, while this problem is alleviated by the proposed method. It can be observed from (b) that the small breakage does not affect the DSC/Recall metric while revealing significant differences in the distance transform map.

alleviated and the TD/BD is increased. However, the over-simplified relaxation of the threshold inevitably degrades the precision and the DSC metric, which is detrimental to the quantitative measurement analysis. This is similar to the over-segment problem introduced by Zheng *et al.* [7]. Instead of using the trivial multi-stage training procedure by [7], the proposed CSL aims to balance the trade-off between the connectivity and overlap-wise measurements via independent objective functions. We first designed a compound loss function embedded with distance prior to adjust the importance of each voxel, reinforcing the network to detect more airway branches. Meanwhile, we maximize the precision at the fixed recall value to deal with the underlying over-segment problem.

Furthermore, the breakage merely induces marginal voxel-level errors but causes the catastrophic structural mistakes. As demonstrated in Fig.1(b), the distance transform can highlight breakage regions and enforce the segmentation result to have the same distance map as the ground-truth. Hence, we propose a Local-Sensitive Distance module (LSD) to repair the broken connection. Concretely, the LSD aims to acquire the binary distance map from the likelihood map via the differentiable operations. Unlike previous works [9], [10] that need to learn the distance transform, we approximate the Euclidean distance from the likelihood map and construct the distance map loss function. The CNNs trained with such loss can enhance the structural connectivity without sacrificing the voxel-wise accuracy.

Overall, the proposed method is an end-to-end framework that does not require a multi-stage training procedure. The two critical components, CSL and LSD cooperate with each other, aiming to facilitate the performance of airway segmentation under multiple evaluation criteria. Extensive experiments on two public pulmonary airway datasets demonstrate that the proposed method has achieved superior performance compared to other state-of-the-art approaches.

## II. RELATED WORK

### A. Evaluation Metrics of Connectivity

The segmentation of tubular-structures requires the specific metrics for evaluating the results. A typical metric is

the Betti-number [11], [12] which measures the connectivity of  $n$ -dimensional simplicial complexes. Among the multiple choices of  $n$ , Betti-0, which considers the number of connected-components, is appropriate for airway segmentation. Another metric is cIDice [13] that focuses more on the skeleton rather than the overall overlapping-accuracy. However, cIDice cannot distinguish the breakages at different locations. For example, the breakages at trachea and the small distal bronchi can lead to the same cIDice while the former cannot be tolerated since it can easily affect the application of the segmentation masks in navigation.

According to [1], [8], TD and BD are designed to measure the connectivity of airway. It should be noticed that both TD and BD are evaluated on the largest component of the prediction results. Therefore, they can fully characterize the properties of Betti-0. Take  $\mathcal{Y}$  and  $\hat{\mathcal{Y}}$  to denote the binary ground-truth label and largest component result of the prediction. TD is defined as the fraction of the tree length that is detected appropriately with regard to the whole tree length in the ground-truth:

$$TD = \frac{T_{det}}{T_{ref}} * 100\%, \quad (1)$$

where the  $T_{det}$  denotes the total length of all airway branches detected in the prediction, and  $T_{ref}$  represents the whole tree length in the ground-truth. BD denotes the percentage of the airway branches that are detected correctly with association to the whole number of branches in the ground-truth:

$$BD = \frac{B_{det}}{B_{ref}} * 100\%, \quad (2)$$

where the  $B_{det}$  denotes the total correct airway branches detected in the prediction, and  $B_{ref}$  represents the whole number of branches in the ground-truth. TD and BD are critical indicators to measure the performance of the automatic airway segmentation algorithms because the connectivity of the airway tree determines the clinical navigation value. However, TD and BD are not friendly to be explicitly optimized via deep learning models since the extraction of the largest component is non-differentiable.

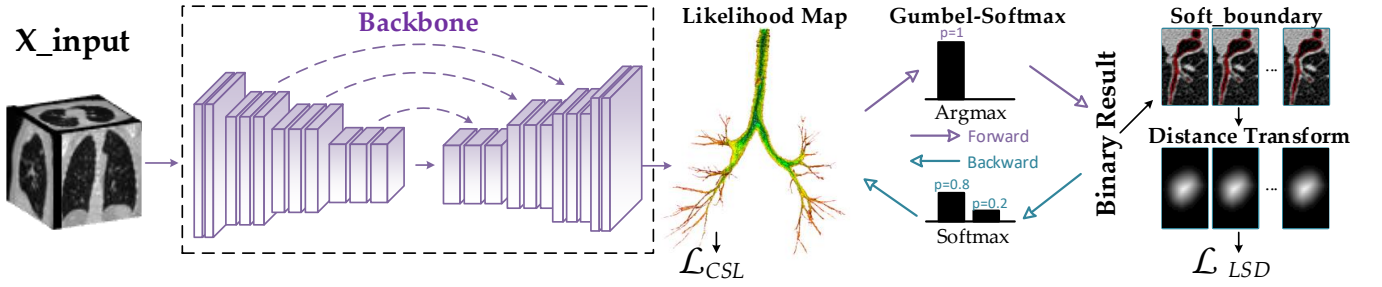


**Fig. 2.** Framework of the proposed connectivity enhancement network. The backbone (3D UNet) generates the likelihood output, followed by two supervised branches that are used to guide the optimization schedule. The first branch is supervised by the Connectivity-Aware Surrogate Loss (CAS) which is designed to simultaneously achieve high completeness and high correctness via independent objective functions. The second branch is the proposed LSD that approximates the Euclidean distance from the likelihood output via differentiable operations. The objective function of LSD is constructed to achieve high airway tree-like structural fidelity without sacrificing the voxel-wise accuracy.

### B. Method of Airway Segmentation

To relieve the burden of manual delineation and help clinicians explore the influence of pneumonia on airways, automatic pulmonary airway segmentation algorithms have been widely explored over the decades. In 2009, EXACT'09 [1] challenge provided a platform for comparing airway extraction algorithms using a public dataset and standard evaluation metrics. During that period, several methods using multi-thresholds [14], template matching [15], and region growing [16] have been proposed to automatically segment the airways. However, these methods often fail in extracting the smaller peripheral bronchi due to the lack of discriminative features.

Recently, the progress of deep learning has promoted the research on airway segmentation. Juarez *et al.* [3] directly adopted 3D CNNs with an elaborated pipeline for automatic airway segmentation. 3D UNet cooperating with the graph refinement [5] and attention mechanism [17] were also proposed to extract more discriminative features. The connectivity of the airway prediction also raises attention. Qin *et al.* [2] proposed the AirwayNet that transformed the binary segmentation task into 26-neighborhood connectivity prediction. Wu *et al.* [18] utilized the long-range slice continuity information. A general union loss (GUL) was designed by Zheng *et al.* [7] to alleviate the within-class distribution imbalance. However, the breakage problem of the airway has not been discussed thoroughly, and the balance between connectivity measurements and overlap-wise accuracy has not been carefully investigated.

## III. METHODS

### A. Problem Formulation and Method Overview

This work addressed the airway segmentation problem.  $\mathbf{x} \in \mathbf{X}$  is the input volume and  $\mathbf{y} \in \mathbf{Y}$  is the ground-truth of segmentation mask. We design a model  $\hat{\mathbf{y}} = \mathcal{F}(\mathbf{x}, \Theta)$  where  $\Theta$  represents the model parameters and  $\hat{\mathbf{y}}$  is the likelihood map of prediction. The model is optimized by loss function  $\mathcal{L}(\hat{\mathbf{y}}, \mathbf{y})$  which measures the difference between the ground-truth and prediction. Fig.2 illustrates the basic procedure of our proposed method. The 3D UNet [19] is deployed as the

backbone followed by two critical components, CSL and LSD. During training procedure, CSL and LSD function upon the likelihood output of the 3D UNet, cooperating to enhance the connectivity of airways and maintain the overlap-wise accuracy.

### B. CAS: Connectivity-Aware Surrogate Loss

The connectivity measurements, TD and BD, are non-differentiable, hence they are hard to be directly optimized through stochastic gradient descent methods. In this work, a Connectivity Surrogate-Aware Loss (CSL) was proposed to enhance the connectivity of airway prediction. We assume that the connectivity simultaneously pursues two goals, high completeness and high correctness. To achieve high completeness means that unconnected regions among bronchi should be repaired. The high correctness represents that the misconnection between the airway and the background should be reduced to alleviate the over-segment problem [7]. Hence, our designed CSL takes both completeness and correctness into consideration.

For one thing, the difficulty of improving the completeness of the pulmonary airway segmentation can be attributed to within-class distribution imbalance. Large airways occupy the majority of foreground voxels, and such imbalanced distribution affects the data-driven deep learning methods, which may lead to poor performance on the peripheral bronchi. To enhance the sensitivity for peripheral airways, we design the following objective function:

$$\mathcal{L}_{com} = \left\{ 1 - \frac{\sum_{i=1}^N \hat{\mathbf{y}}_i \mathbf{y}_i}{\alpha_t \sum_i \hat{\mathbf{y}}_i + \beta_t \sum_i \mathbf{y}_i} \right\} + \left\{ \sum_{i=1}^N \alpha_i \text{CE}(\hat{\mathbf{y}}_i, \mathbf{y}_i) \right\}. \quad (3)$$

The first term of Eq.(3) is the Tversky loss [20], where  $\alpha_t + \beta_t = 1$ . Both  $\alpha_t$  and  $\beta_t$  are hyperparameters to balance the recall and sensitivity of segmentation. Further, the gradients of different airway voxels should vary with the branch sizes during backward propagation. Therefore, the tubular radius prior is integrated into the Cross-Entropy (CE) loss function, as seen in the second term of Eq.(3), to further resolve the within-class distribution imbalance. The  $\alpha$  is the distance-based

weighting map. The weight of each airway voxel depends on the Euclidean distance to the centerline, which is defined as:

$$\alpha_i = \begin{cases} -\lambda_{fg} \log(\frac{dc_i}{dc_{max}} + \varepsilon), & \mathbf{y}_i = 1, \\ 1, & \mathbf{y}_i = 0, \end{cases} \quad (4)$$

where the  $dc_i$  is the shortest Euclidean distance from its location to the centerline,  $dc_{max}$  is the maximum of  $dc_i$  in one sample.  $\lambda_{fg}$  is the weighting factor and  $\varepsilon$  is a small positive number to avoid the numerical error.  $\mathcal{L}_{com}$  is designed to dynamically pay more attention to the challenging regions. Fig.3 shows the weight profiles of the main bronchus and peripheral bronchus, which is consistent to Eq.(4).

For another, previous work [4], [8] observed that enhancing the completeness of the pulmonary airway may decrease the overlap-wise accuracy. The underlying cause of this phenomenon is over-segmenting the airway. Although some post-processing techniques [21] could alleviate this problem, they add extra trivial parameters tuning tasks that reduce the efficiency of the models. In this work, we design a correctness surrogate termed as  $\mathcal{L}_{cor}$ . It maximizes the precision at the fixed recall value, thereby reducing the misconnection between the airway and background.  $\mathcal{L}_{cor}$  aims to achieve a satisfactory trade-off between completeness and correctness. The  $\mathcal{L}_{cor}$  is embedded in the whole end-to-end training procedure with the simple warm up technique. The Label Space  $\mathcal{Y}$  contains the positive examples:  $\mathcal{Y}^+$ , and the negative examples:  $\mathcal{Y}^-$ . The results of the model prediction are categorized into four components: true positive (TP), true negative (TN), False Positive (FP), and False Negative (FN).  $\mathcal{Y}^+$  contains the TP and FN, and  $\mathcal{Y}^-$  contains the TN and FP. The concrete definitions that combine with the model can be seen as follows:

$$\begin{aligned} TP &= \sum_{i \in \mathcal{Y}^+} \mathbb{1}[\mathcal{F}(\Theta; \mathbf{x}_i) \geq T] \\ &= \sum_{i \in \mathcal{Y}^+} 1 - \mathcal{L}_{zero\_one}(\mathcal{F}(\Theta; \mathbf{x}_i, T), \mathbf{y}_i) \end{aligned} \quad (5)$$

where the  $\mathcal{L}_{zero\_one}$  denotes the Zero-One loss function. Similarly,  $FP = \sum_{i \in \mathcal{Y}^-} \mathcal{L}_{zero\_one}(\mathcal{F}(\Theta; \mathbf{x}_i, T), \mathbf{y}_i)$ . As shown in Fig.3, a series of precision at fixed recall values are maximized by the  $\mathcal{L}_{cor}$ . The precision is defined as  $P = [TP / (TP + FP)]$  and the recall is  $R = [TP / (TP + FN)]$ . We first define the preliminary optimization problem: Maximize the precision at the fixed recall value of  $\delta$ , denoted by  $P@R_\delta$ :

$$\begin{aligned} P@R_\delta &= \max_{\mathcal{F}_\Theta} \frac{TP}{TP + FP} \\ &\text{s.t. } \frac{TP}{|\mathcal{Y}^+|} \geq \delta, \end{aligned} \quad (6)$$

where  $\mathcal{Y}^+$  is the total account of the positive examples. Since the  $\mathcal{L}_{zero\_one}$  is non-convex and hard to be optimized by SGD algorithms, we choose the hinge loss as a natural replacement, and the TP and FP should be bounded as follows:

$$\begin{aligned} TP &= \sum_{i \in \mathcal{Y}^+} 1 - \mathcal{L}_{zero\_one}(\mathcal{F}(\Theta; \mathbf{x}_i, T), \mathbf{y}_i) \\ &\geq \sum_{i \in \mathcal{Y}^+} 1 - \mathcal{L}_{hinge}(\mathcal{F}(\Theta; \mathbf{x}_i, T), \mathbf{y}_i) = TP^l, \end{aligned} \quad (7)$$

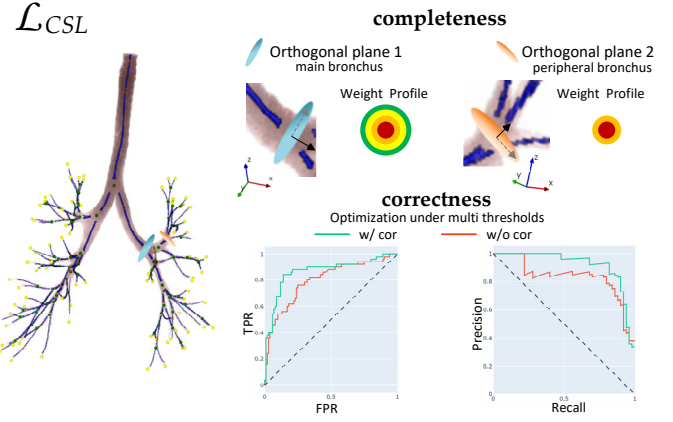


Fig. 3. The CAS module enhances the connectivity via pursuing high completeness and correctness. For completeness, we set different weight profiles by considering the radius of airway branches. For correctness, we maximize a series of precision at fixed recall values to improve the accuracy with multiple thresholds.

where the  $\mathcal{L}_{hinge}(\mathcal{F}(\Theta; \mathbf{x}_i, T), \mathbf{y}_i) = \max\{0, 1 - \mathbf{y}_i[\mathcal{F}_\Theta(\mathbf{x}_i) - T]\}$ ,  $TP^l$  is the lower bound of the TP, similarly,  $FP \leq \sum_{i \in \mathcal{Y}^-} \mathcal{L}_{hinge}(\mathcal{F}(\Theta; \mathbf{x}_i, T), \mathbf{y}_i) = FP^u$ .  $FP^u$  is the upper bound of the FP. Then the objective of the Eq.(6) can be transformed as follows:

$$\begin{aligned} \widehat{P@R}_\delta &= \min_{\mathcal{F}_\Theta} -\frac{\delta |\mathcal{Y}^+|}{\delta |\mathcal{Y}^+| + FP^u} \\ &\text{s.t. } \frac{TP^l}{|\mathcal{Y}^+|} - \delta \geq 0 \end{aligned} \quad (8)$$

We apply the Lagrange multiplier to obtain the equivalent objective function:

$$\widehat{P@R}_\delta = \min_{\mathcal{F}_\Theta} \max_{\nu \geq 0} -\frac{\delta |\mathcal{Y}^+|}{\delta |\mathcal{Y}^+| + FP^u} + \nu \left( \frac{TP^l}{|\mathcal{Y}^+|} - \delta \right), \quad (9)$$

where  $\nu$  is a Lagrangian multiplier and Eq.(9) can be solved by SGD algorithm, iteratively updating  $\Theta$  and  $\nu$ . Hence, the final  $\mathcal{L}_{cor}$  is defined by:

$$\mathcal{L}_{cor} = \min_{\mathcal{F}_\Theta} - \sum_{k=1}^m (\delta_k - \delta_{k-1}) \widehat{P@R}_{\delta_k}, \quad (10)$$

where  $\delta_k = \delta_0 + \frac{(1-\delta_0)k}{m}$ ,  $\delta_0$  is the positive class prior. The  $\mathcal{L}_{cor}$  cooperating with the  $\mathcal{L}_{com}$  aids in enhancing the connectivity of the pulmonary airway, the CAS loss function is finally defined as:

$$\mathcal{L}_{CAS} = \lambda_1 \mathcal{L}_{com} + \lambda_2 \mathcal{L}_{cor}, \quad (11)$$

where  $\lambda_1$  and  $\lambda_2$  are empirically set  $\lambda_1 = \lambda_2 = 1$  in our work.

### C. LSD: Local-Sensitive Distance Loss

In addition to the proposed CAS that functions at the voxel level to enhance the connectedness, we found that, compared with the binary segmentation masks, distance transform maps can highlight the region-wise structural features by measuring the distance between voxels to the nearest boundary. As shown in Fig.1, the local breakage can be easily observed by this map even if it has slight impacts on overlap-wise metrics.

Recent studies have demonstrated that introducing distance transform maps into CNNs could boost the performance of medical image segmentation [22]–[24]. However, these methods mainly suffer two drawbacks: 1) It is intractable to directly regress the Signed Distance Map (SDM), especially for the complicated airway tree structure. 2) The commonly used distance transform is non-differentiable, therefore it is difficult to unify the distance transform map with the network in an end-to-end fashion. In this paper, we introduce a novel LSD module to build a differentiable distance transform as a loss function, collaborating with the CAS Loss to improve the topological connectivity of the pulmonary airway. The core challenge of LSD is to determine the foreground voxels in the likelihood map and then calculate the shortest distance from all inside foreground voxels to their boundary. To tackle such a problem, a sequential procedure is designed to construct LSD. Concretely, the **Likelihood** map is first reparameterized by **Gumbel-softmax**, then **Soft\_boundary** extraction by pooling functions, and finally **Distance** transform via the Euclidean distance filled kernel. Given that each component of LSD is differentiable, therefore the overall gradient flow is guaranteed.

Firstly, the gumbel-softmax [25] is used as an alternative to discarding the argmax gate. The logits of likelihood map  $\hat{y}$  can be converted into the binary result and the gradient map through gumbel-softmax is computed identically to the ones through softmax. Specifically,  $\hat{y} = [\hat{y}^1; \hat{y}^2]$  contains two maps, where  $\hat{y}^1$  and  $\hat{y}^2$  denote the likelihood map of background and foreground respectively. The gumbel-softmax distribution adopts softmax as a continuous relaxation to argmax, hence, we can acquire the binary result  $\hat{z}$  via the differentiable equation:

$$\hat{z}^i = \frac{\exp(\log((\hat{y}^i) + g^i)/\tau)}{\sum_{j=1}^2 \exp(\log((\hat{y}^j) + g^j)/\tau)}, \text{ for } i = 1, 2. \quad (12)$$

where  $\hat{g}^i$  represents the standard Gumbel distribution:  $g = -\log(-\log(u))$  with  $u$  sampled from a uniform distribution, i.e.,  $u \sim \text{Unif}[0, 1]$ .  $\tau$  is the temperature parameter that controls the discreteness of the binary result  $\hat{z}$ . When  $\tau$  becomes closer to 0, the samples from the Gumbel Softmax distribution become almost the same as the one-hot argmax output. We set  $\tau = 0.1$  in practical use, which is effective enough for the accuracy of experiments.

Secondly, the binary result  $\hat{z}$  is composed of the foreground map  $\hat{z}^{\text{fg}} = \hat{z}^2$  and the background map  $\hat{z}^{\text{bg}} = \hat{z}^1$ . We simulate the morphological erosion and dilation operations via the max\_pooling function to construct the soft\_erosion and soft\_dilation. These operations are key components to extracting the boundary of the foreground map  $\partial \hat{z}^{\text{fg}}$ :

$$\partial \hat{z}^{\text{fg}} = [\text{soft\_dilation}(\hat{z}^{\text{fg}}) - \text{soft\_erosion}(\hat{z}^{\text{fg}})] \odot y. \quad (13)$$

Thirdly, we introduce the kernel-based method to solve the distance transform of the  $\hat{z}^{\text{fg}}$ . The key step is to solve the shortest distance from each voxel in the  $\hat{z}^{\text{fg}}$  to the boundary  $\partial \hat{z}^{\text{fg}}$ , which can be defined as:

$$\text{Dist}(\hat{z}^{\text{fg}}) = \min_{\forall \varphi \in \partial \hat{z}^{\text{fg}}} d(\hat{z}^{\text{fg}}, \varphi), \quad (14)$$

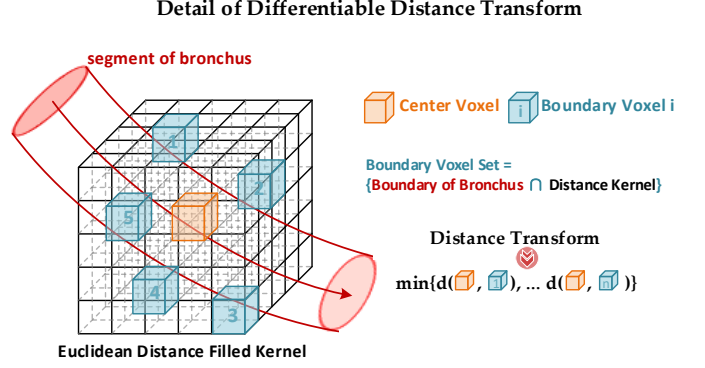


**Fig. 4.** Illustration of detail of differentiable distance transform. The shortest distance between the center voxel and the boundary voxel set is calculated based on the Euclidean distance filled kernel.

where  $d(\cdot, \cdot)$  denotes the Euclidean distance. Take one voxel  $p \in \hat{z}^{\text{fg}}$  and  $\varphi \in \partial \hat{z}^{\text{fg}}$  as example,  $d(p, \varphi) : \mathbb{R}^3 \rightarrow \mathbb{R}_0^+$  can be defined as:

$$d(p, \varphi) = d(p - \varphi, 0) = d(p - \varphi) = \|p - \varphi\|_2 \quad (15)$$

The question now is transformed to distinguish the shortest distance from the distance set via differentiable computation. The distance set for a single voxel  $p$  contains:  $\{d_1, d_2, \dots, d_n\} = \{d(p, \varphi_1), d(p, \varphi_2), \dots, d(p, \varphi_n)\}$ . A convolutional kernel is initialized with the Euclidean distance value to the centroid, vividly seen in Fig.4, the size of Euclidean distance filled kernel is set to  $31 \times 31 \times 31$ , which guarantees the airway voxels could touch the boundary. The property of the log-sum-exponential [26] can smoothly approximate the minimum/maximum of two real variables. Pham *et al.* [27] leveraged this theory to calculate the transformation of the background in 2D images. However, their representation ability was limited due to the truly useful distance transform of the foreground cannot be acquired. Moreover, the transformation of the background in 3D images is impractical due to the GPU memory capability. We construct the reliable distance transform of the airway on top of the log-sum-exponential. The problem is reformulated as:

$$LSE_\beta(d_1, \dots, d_n) = \frac{1}{\beta} \log(\exp(\beta d_1) + \dots + \exp(\beta d_n)) \quad (16)$$

Without loss of generality, we can assume that  $\{d_1 = d_2 = \dots = d_k < d_{k+1} \leq \dots d_n\}$ , and *Lemma 1* derives the minimum distance.

$$\text{Lemma 1: } \min\{d_1, d_2, \dots, d_n\} = \lim_{\beta \rightarrow -\infty} LSE_\beta(d_1, \dots, d_n)$$

Detailed proof can be seen in Appendix. Finally, the distance transform are concluded as:

$$\begin{aligned} \text{Dist}(\hat{z}^{\text{fg}}) &= \lim_{\beta \rightarrow -\infty} \frac{1}{\beta} \log(\partial \hat{z}^{\text{fg}} \cdot \exp(\beta d(\hat{z}^{\text{fg}} - \varphi))), \\ &= \lim_{\beta \rightarrow -\infty} \frac{1}{\beta} \log(\partial \hat{z}^{\text{fg}} * \exp(\beta d(\hat{z}^{\text{fg}}))), \\ &= \lim_{\gamma \rightarrow 0} \gamma \log(\partial \hat{z}^{\text{fg}} * \exp(\frac{1}{\gamma} d(\hat{z}^{\text{fg}}))), \end{aligned} \quad (17)$$

where the  $*$  is the convolutional operator, and  $\gamma = \frac{1}{\beta}$ . We set  $\gamma = -0.3$  in experiments that enable the smooth approximation of the LSD. Since all components are differentiable, the proposed LSD could be integrated as a differentiable distance transform layer into the end-to-end training framework. Given that the distance transform map of the likelihood map is obtained, we further design a distance map loss that penalizes the false predictions from the global perspective:

$$\mathcal{L}_{LSD} = \omega \cdot \|\text{Dist}(\mathbf{y}) - \text{Dist}(\hat{\mathbf{z}}^{\text{fg}})\|_2, \quad (18)$$

where the  $\omega$  is a weighting balance to handle the imbalance between the foreground and the background.

$$\omega = \begin{cases} \frac{N_{\text{bg}}}{N_{\text{fg}}}, & \text{if foreground,} \\ 1, & \text{otherwise.} \end{cases} \quad (19)$$

where the  $N_{\text{fg}}$  and  $N_{\text{bg}}$  denote the number of voxels in the foreground and background, respectively. In conclusion, the proposed connectivity enhancement network owns two critical modules, the CAS and LSD. These two modules cooperate with each other to enhance the connectedness of the pulmonary airway.

## IV. EXPERIMENTS

### A. Datasets

Two public datasets are used for evaluation in our work. 1) **The EXACT'09 Challenge** [1]. It provides 20 CT scans for training and 20 CT scans for testing, however no airway annotation is public available. All CT scans share an axial size of  $512 \times 512$ , with a spatial resolution ranging from 0.5 mm to 0.78 mm. The quantity of the axial slices varies from 157 to 764 and their slice thickness ranges between 0.45 mm to 1.0 mm. 2) **The Binary Airway Segmentation Dataset (BAS)** [17]. The BAS contains 90 CT scans with airway annotation. The spatial resolution ranges from 0.5 mm to 0.82 mm and the slice thickness ranges from 0.5 mm to 1.0 mm. For the BAS dataset, we randomly split the 90 CT scans into the training set (50 scans), validation set (20 scans), and test set (20 scans). The model trained on the BAS dataset was used to evaluate on the test set of the EXACT'09 challenge. For a fair comparison, the resulting binary segmentations were submitted to the organizers who sent the quantitative evaluations back.

### B. Implementation Details

**Network Configuration and Data Preprocessing:** As shown in the Fig.2, 3D UNet was chosen as the backbone with a slight modification, each block in the encoder or decoder contains two convolutional layers followed by Instance Normalization [28] and pReLU [29]. Initial channel number was set to 32. During the preprocessing procedure, we clamped the voxel values to  $[-1000, 600]$  Hounsfield Unit, normalized them into  $[0, 255]$ , and cropped the lung field to remove unrelated background regions.

**Optimization Procedure:** We adopted a large input size of  $128 \times 224 \times 304$  CT cubes densely cropped near airways and chose a batch size of 1 in the training phase. On-the-fly data augmentation included the random horizontal flipping and

---

### Algorithm 1 Main optimization procedure.

---

**Input:** input  $\mathbf{x}$ , label  $\mathbf{y}$ , current epoch  $T_c$ , warm up epoch  $T_w$ .  
 Initialize the backbone  $\mathcal{F}_\Theta$ .  
**while** not converged **do**  
 Acquire likelihood map  $\hat{\mathbf{y}}$  from  $\mathcal{F}_\Theta$ ,  $\hat{\mathbf{y}} = \mathcal{F}_\Theta(\mathbf{x})$ .  
 if  $T_c < T_w$ :  
 Compute  $\mathcal{L}_{\text{com}}(\hat{\mathbf{y}}, \mathbf{y})$ .  
 Update  $\Theta$  with  $\mathcal{L}_{\text{com}}$ .  
 else:  
 Compute  $\mathcal{L}_{\text{com}}(\hat{\mathbf{y}}, \mathbf{y})$ .  
 Compute  $\mathcal{L}_{\text{cor}}(\hat{\mathbf{y}}, \mathbf{y})$ .  
 Use Gumbel-Softmax to obtain  $\hat{\mathbf{z}}^{\text{fg}}$  from  $\hat{\mathbf{y}}$ .  
 Use morphological operations to get  $\partial \hat{\mathbf{z}}^{\text{fg}}$  from  $\hat{\mathbf{z}}^{\text{fg}}$ .  
 Calculate the distance transform of  $\mathbf{y}$  and  $\hat{\mathbf{z}}^{\text{fg}}$  via the LSD,  $\text{Dist}(\mathbf{y})$  and  $\text{Dist}(\hat{\mathbf{y}})$ . Then compute distance map loss,  $\mathcal{L}_{\text{LSD}}(\text{Dist}(\hat{\mathbf{y}}), \text{Dist}(\mathbf{y}))$ .  
 Update  $\Theta$  with  $\mathcal{L}_{\text{com}} + \mathcal{L}_{\text{cor}} + \mathcal{L}_{\text{LSD}}$ .  
**end**

---

random rotation between  $[-10^\circ, 10^\circ]$ . Adam optimizer was used with the initial learning rate of 0.002. The total epoch was set to 60, the first ten epochs were used as warm up solution. The learning rate was divided by 10 in the 50<sup>th</sup> epoch. We chose  $\alpha_t = 0.1$ ,  $\lambda_{\text{fg}} = 10$ ,  $\delta = 0.8$ , and  $m = 10$  in the CAS module via experimental results. The detailed training optimization of the proposed network can refer to the [Algorithm.1](#). During the testing phase, we performed the sliding window prediction with stride 48. The results were averaged on the overlapping regions and a threshold ( $th = 0.5$ ) function was used to obtain the final binary segmentation results. The proposed model took around 12 seconds to predict a sub-volume CT cube with the size of  $128 \times 224 \times 304$ . We adopted the PyTorch framework to implement all experiments, which were executed on a linux workstation with Intel Xeon Gold 5218 CPU @ 2.30 HZ, 128 GB RAM, and 2 NVIDIA Geforce RTX 3090 GPUs.

**Evaluation Metrics:** Following the state-of-the-art methods [7], [8], TD and BD were chosen as the connectivity measurements for all experiments. As for the voxel-wise accuracy, Specificity (Spe, %) was evaluated by EXACT'09 [1], we also included this metric for the BAS dataset. To measure the overlap-wise accuracy, we provided the generation-wise DSC metrics in the BAS dataset because it has fine-grained annotation of the airways while EXACT'09 does not. The generation-wise DSC metrics are calculated within the generation of airway branches according to their diameters. The motivation of generation-wise DSC is to reveal the performance achieved by different algorithms on different generations of airway, especially the peripheral airways. The quantitative measurement of the peripheral airways are clinical significant while the global DSC could not reflect the performance because their voxel occupation is far fewer than the trachea and main bronchi.

### C. Quantitative Results Analysis

The results of the EXACT'09 Challenge test data are reported in the [Table I](#). It is observed that our proposed method

TABLE I

COMPARISON IN THE EXACT-09 DATASET. THE RESULTS ARE REPORTED IN THE FORMAT OF MEAN  $\pm$  STANDARD DEVIATION. ALL RESULTS ARE ACQUIRED FROM THE OFFICIAL ORGANIZATION. FOR SIMPLICITY, 'BD' REPRESENTS BRANCH DETECTED, 'TD' REPRESENTS TREE LENGTH DETECTED, AND 'SPE' REPRESENTS SPECIFICITY.

Method	BD (%) $\uparrow$	TD (%) $\uparrow$	Spe(%) $\uparrow$
Neko <sup>†</sup>	35.5 $\pm$ 8.2	30.4 $\pm$ 7.4	99.11 $\pm$ 1.78
Murphy <i>et al.</i> [30]	41.6 $\pm$ 9.0	36.5 $\pm$ 7.6	<b>99.29 <math>\pm</math> 1.67</b>
Xu <i>et al.</i> [31]	51.1 $\pm$ 10.9	43.9 $\pm$ 9.6	93.22 $\pm$ 26.60
MISLAB <sup>†</sup>	42.9 $\pm$ 9.6	37.5 $\pm$ 7.1	<u>99.11 <math>\pm</math> 1.64</u>
Smistadet <i>et al.</i> [32]	31.3 $\pm$ 10.4	27.4 $\pm$ 9.6	96.40 $\pm$ 3.37
Qin <i>et al.</i> [8]	76.7 $\pm$ 11.5	72.7 $\pm$ 11.6	96.35 $\pm$ 2.86
Zheng <i>et al.</i> [7]	80.5 $\pm$ 12.5	79.0 $\pm$ 11.1	94.21 $\pm$ 4.25
Proposed	<b>82.1 <math>\pm</math> 10.6</b>	<b>79.6 <math>\pm</math> 9.5</b>	93.68 $\pm$ 4.55

<sup>†</sup> Directly use the name of the participant team.

achieved the highest performance on the metric of BD (82.1%) and the second-highest performance on TD (79.6%). Compared with other methods [17], [33], our approach improved the connectivity of the airway without sacrificing too much voxel-wise accuracy. Specifically, Inoue *et al.* [34] designed the multi-stages framework for airway extraction. Although they achieved the highest TD (79.9%), the side-effect was also conspicuous, as the Spe decreased to 88.18%. Our approach could obtain similar high TD (79.6%) while maintaining the acceptable Spe (93.68%). Further, on the metric of branch detected rate, we achieved 82.1% BD, which had 2.5 percentage points higher than the method of Inoue. This observation reveals that the proposed method had truly detected more different bronchi rather than extending the length of partial bronchi. Our method also performed better than the recent submission on the EXACT'09 [7], [8]. Compared with the 76.7% BD and 72.7% TD achieved by Qin, we obtained a higher performance of 82.1% BD and 79.6% TD, which demonstrated that the connectivity of the airway was better preserved by our methods. Zheng *et al.* adopted the WingsNet [7] as the backbone, designing GUL function to resolve the airway segmentation. Compared to their results, our approach revealed better capability in enhancing the connectivity of the airways, + 1.6% BD, + 0.6% TD, with only a slight decrease of the Spe (approximately + 0.5%).

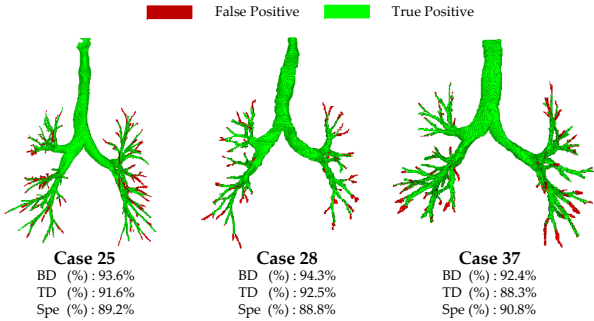


Fig. 5. Three cases with the lowest Spe in the EXACT'09 test dataset are presented. The green represents the true positive and the red denotes the false positive (best viewed in color). The false positives are almost the distal bronchi. No significant mass of leakage is observed.

TABLE II

COMPARISON IN THE BINARY AIRWAY SEGMENTATION DATASET. THE RESULTS ARE REPORTED IN THE FORMAT OF MEAN  $\pm$  STANDARD DEVIATION.

Method	TD (%) $\uparrow$	BD (%) $\uparrow$	Spe(%) $\uparrow$
Juarez <i>et al.</i> 2018 [3]	84.12 $\pm$ 9.15	74.15 $\pm$ 13.5	99.983 $\pm$ 0.009
Juarez <i>et al.</i> 2019 [4]	84.85 $\pm$ 8.67	75.33 $\pm$ 12.4	<b>99.986 <math>\pm</math> 0.010</b>
Qin <i>et al.</i> 2019 [2]	84.16 $\pm$ 10.4	78.45 $\pm$ 9.51	<b>99.986 <math>\pm</math> 0.009</b>
Qin <i>et al.</i> 2021 [8]	<b>90.89 <math>\pm</math> 5.42</b>	87.51 $\pm$ 9.94	99.965 $\pm$ 0.014
Isensee <i>et al.</i> 2021 [34]	84.34 $\pm$ 7.59	85.87 $\pm$ 5.83	99.982 $\pm$ 0.011
Wu <i>et al.</i> 2022 [18]	87.59 $\pm$ 8.71	79.83 $\pm$ 11.4	99.970 $\pm$ 0.017
DDT (CVPR, 2020) [24]	89.51 $\pm$ 6.91	84.53 $\pm$ 5.18	99.976 $\pm$ 0.010
clDice (CVPR, 2021) [13]	88.45 $\pm$ 7.59	86.67 $\pm$ 5.83	99.979 $\pm$ 0.009
GUL (TMI, 2021) [7]	89.27 $\pm$ 7.73	<u>88.10 <math>\pm</math> 6.23</u>	99.958 $\pm$ 0.018
Proposed	<b>96.52 <math>\pm</math> 3.95</b>	<b>91.50 <math>\pm</math> 2.99</b>	99.951 $\pm$ 0.018

The highest Spe (99.29%) was achieved by Murphy *et al.*, however, their BD and TD were striking low, only had 41.6% BD and 36.5% TD. It can be certainly deduced that they can only detect the large airways while missing the majority of the small airway branches, leading to the poor performance on the connectivity. Only the airway prediction with excellent connectivity share the function of the guidance for the bronchoscopic-assisted surgery. Hence, it is utterly useless to have high Spe without the high TD/BD. On the contrary, our proposed method achieved the excellent TD/BD, meanwhile obtained the acceptable Spe. Besides, since EXACT'09 did not have fine-grained annotation of the airways, the part of prediction that considered as false positives could be true distal airways that detected by our method while neglected by the experts. As seen in the Fig.5, no severe clumps of leakage of the airway were observed in the EXACT'09 results.

The experimental results in BAS dataset, reported in Table II, were broadly similar to those in EXACT'09 Challenge test data. First, some state-of-the-art airway segmentation algorithms [2]–[4], [17] were re-implemented for comparison. Juarez *et al.* [3] trained a 3D UNet with a compound loss function to automatically segment airways. Further, they replaced the bottleneck layer with a Graph Neural Network (GNN) module. The results showed they achieved high DSC performance but failed to detect the small bronchi. Qin *et al.* designed the AirwayNet [2] to predict the connectivity of airways. With the integration of feature recalibration and attention distillation, the TD and BD could increase from 84.16% and 78.45% to 90.89% and 87.51%, respectively. We also implemented the nnUNet [34] since it has established very strong baselines for medical image segmentation tasks. The TD (84.32%) and BD (85.87%) achieved by nnUNet are relatively low, which demonstrates the necessity to develop new components for improving the tubular structures. Wu *et al.* [18] introduced a long-term slice propagation to capture long-term continuity information. However, the enhancement is limited since the propagation directions had not been exploited to the full. DDT [24], clDice [13], and GUL [7] designed specific loss functions for airway tree-like tubular structures, which are the most relevant to our work. DDT [24] combined the CNN with the level-set functions, rephrasing the distance

TABLE III

COMPARISON OF GENERATION-WISE DSC IN THE BINARY AIRWAY SEGMENTATION DATASET. THE RESULTS ARE REPORTED IN THE FORMAT OF MEAN  $\pm$  STANDARD DEVIATION.

Method	[0-2](mm, ~40%)	[2-4](mm, ~46%)	[4-6](mm, ~8%)	[6-8](mm, ~3%)	[8-20](mm, ~3%)
DDT [24]	22.90 $\pm$ 11.24	44.21 $\pm$ 6.93	65.11 $\pm$ 3.53	<b>82.59 <math>\pm</math> 4.06</b>	<b>93.03 <math>\pm</math> 1.94</b>
clDice [13]	38.11 $\pm$ 8.84	51.25 $\pm$ 7.97	69.53 $\pm$ 3.31	82.44 $\pm$ 11.99	92.85 $\pm$ 2.51
GUL [7]	45.42 $\pm$ 4.97	60.62 $\pm$ 4.21	<b>72.21 <math>\pm</math> 6.90</b>	79.40 $\pm$ 4.38	90.62 $\pm$ 3.06
Proposed	<b>50.12 <math>\pm</math> 4.20</b>	<b>64.19 <math>\pm</math> 5.43</b>	70.15 $\pm$ 4.11	80.01 $\pm$ 4.91	91.47 $\pm$ 2.48

prediction problem as a classification problem based on quantization. Unfortunately, the Geometry-aware Refinement (GAR) in DDT is non-differentiable and adds an extra burden to the optimization procedure. The clDice loss function [13] handled the false positive and false negative samples simultaneously. It emphasized the connectivity via the calculation of the soft-skeleton, however, the iterative pooling operations they adopted cannot accurately extract 3D soft-skeleton. Moreover, TD/BD is calculated after the largest component extraction of the prediction while clDice not, hence the clDice cannot perform synchronously as TD/BD. GUL [7] was proposed to give large weights to the centerline of airways, while it needed hard-to-segment region prior, and it may fall into the over-segment problem. Compared with these methods, our method demonstrated the remarkable superiority in enhancing the connectivity of the airway. Our method outperformed theirs by more than 7% on the TD, + 7.25% compared to DDT, + 8.07% to clDice, and + 7.01% to GUL. The improvement on BD was also noticeable. It is increased by 6.97%, 4.83%, and 3.40% compared to the DDT, clDice, and GUL respectively.

The proposed method achieved the best performance on the connectivity measurements while maintaining the competitive voxel-wise/overlap-wise accuracy. Table II showed that all methods achieved high performance on the Spe (more than 99.9%), and to investigate deeper on the comparison of the overlap-wise accuracy, we conducted the experiments of the generation-wise DSC, which was reported in Table III. The large airways whose diameter larger than 6mm accounted for a very small portion, only about 6%. 3% of them lie in the interval of [6-8] mm, and the rest are larger than 8 mm. The majority of the airway branches own the diameters between [0-4] mm, occupying more than 80% branches ([0-2] mm and [2-4] mm account for 40% and 46%, respectively). Our approach performed much better than counterparts with regard to the majority of the airway branches. We achieved 50.12% DSC on the airways of [0-2]mm and 64.19% DSC of [2-4]mm, which exceeded to a large extent compared to other methods. It corroborated that our approach can enhance the connectivity of the airway while maintaining the competitive overlap-wise accuracy. The only deficiency is that the DSC performance on the larger airways is a bit lower than DDT and clDice. Fortunately, the decrease of 2% DSC on the large airways was acceptable, and the morphological shape of them were not changed as seen in visualization of Fig.5 and Fig.6. In addition, large airways share a small proportion of the total branches, and they are less significant in clinical usage than the peripheral airways.

TABLE IV

ABLATION STUDY OF THE PROPOSED METHOD ON THE BAS DATASET.

CAS	LSD	TD(%) $\uparrow$	BD(%) $\uparrow$	Spe(%) $\uparrow$
✓		95.44 $\pm$ 3.92	90.50 $\pm$ 3.01	99.938 $\pm$ 0.021
	✓	92.60 $\pm$ 7.60	89.38 $\pm$ 6.26	99.956 $\pm$ 0.020
✓	✓	96.52 $\pm$ 3.95	91.50 $\pm$ 2.99	99.951 $\pm$ 0.018

#### D. Qualitative Results Analysis

For the EXACT'09 Challenge test data, we presented three cases with inferior Spe in Fig.5. It can be seen that almost all false positives belong to the distal airways, which may be not annotated by the experts. No severe clumps of leakage of the airway were observed in the EXACT'09 results.

For the BAS dataset, compared with other methods developed for tubular structures, Fig.6 demonstrated the effectiveness and robustness of our approach. All the airway prediction results were post-processed by the largest component extraction. In line with the Table II, all methods segmented main bronchi well, however, our method preserved the peripheral airway structures more precisely than others, as seen in the local details of Case 1 in the Fig.6. In addition, local details of Case 2 showed that our method can detect as many as possible of distal airways. These observations substantiate that the proposed connectivity enhancement network could identify the breakage phenomenon with superior sensitivity and preserve the connectivity of the airway tree.

## V. DISCUSSIONS

### A. Impacts of Individual Modules

The ablation study on the proposed method was conducted. Table IV reports the impacts of individual modules. The LSD is designed to be sensitive to the breakage phenomenon and constructed the corresponding loss function to enhancing the connectivity of the airway without sacrificing voxel-wise accuracy. It improved the performance to 92.60% TD, 89.38% BD, and 99.956% Spe. The CAS module can improve the connectivity measurement to 95.44% TD and 90.50% BD. The Sep slightly decreased to 99.938%. Combined with the CAS and LSD, we obtained the final best performance, 96.52% TD, 91.50% BD, and 99.951% Spe. The likelihood map of three profiles in Fig.7 vividly revealed that the proposed method can assign proper likelihoods for within-class imbalanced airways to alleviate the breakage problems. Further, compared with the methods with completeness objective function, the false positives are reduced by the proposed approach, as shown in the false positive rendering in Fig.7.

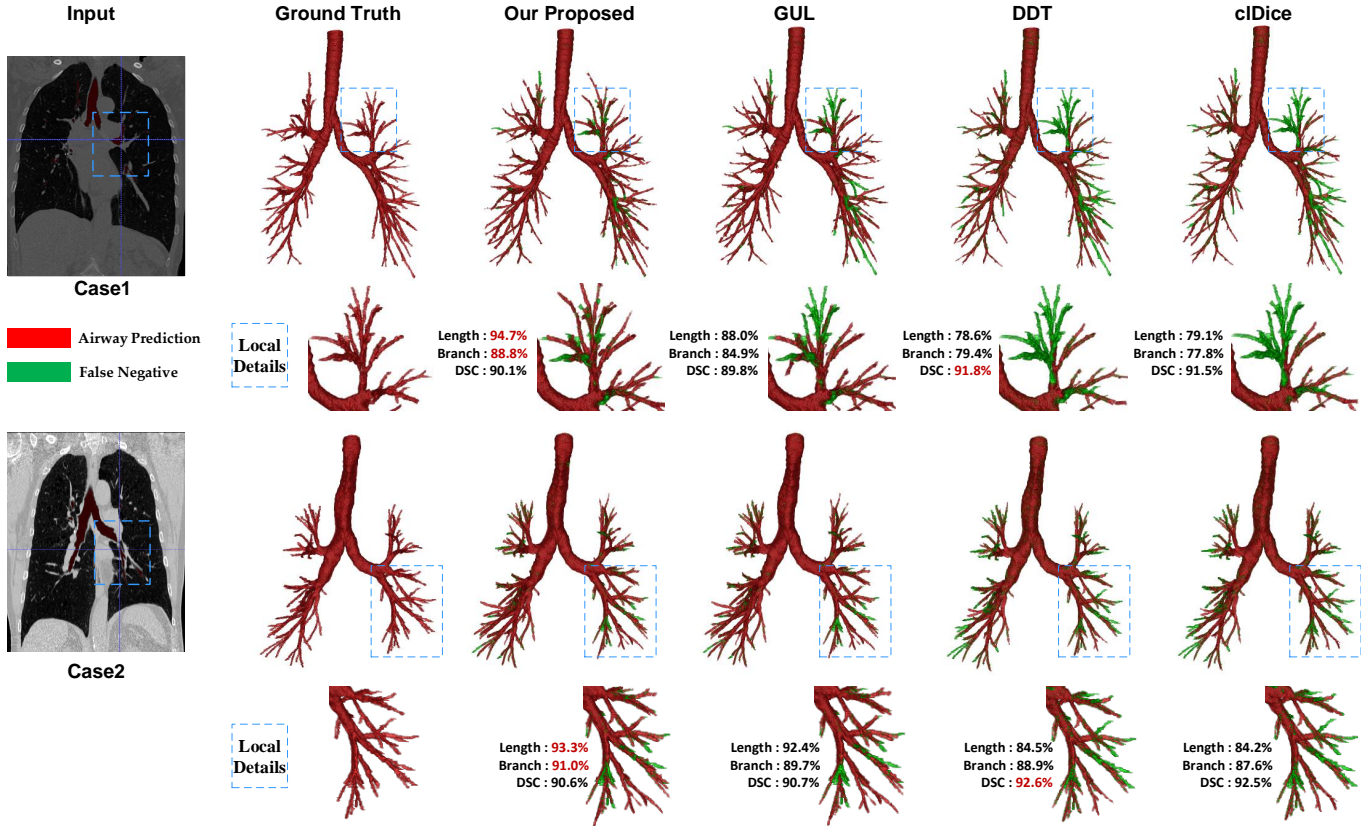


**Fig. 6.** Visualization of the segmentation results of the proposed approach and compared methods. Only the largest component of the predictions are rendered in red. The green part reveals the false positives compared to the ground-truth. Blue dotted boxes represent local details of airway results. Best viewed in color and magnified.

### B. Rethinking Tree-like Structure Priors in Deep Learning Era

This work designed differentiable modules, CAS and LSD, to improve connectivity of airway segmentation. The tree-like structure priors, including the local smoothness, connectivity, and other issues, have been widely investigated in medical imaging computing since segmenting objects while preserving their global structures are important for clinical diagnosis. Previous works have formulated these issues as implicit or explicit constraints during the model optimization. Thanks to the development of deep learning and the increasing size of clinical data, we can easily train a neural network via minimizing the differences between predictions and the ground-truth. However, the loss term should be differentiable since the stochastic optimization and back-propagation are deployed to update the parameters of models. DSC metric (and its variants) is differentiable and plays an important role in segmentation tasks since it can be used for both model training and evaluation. Despite the high voxel-wise accuracy achieved by DSC objective function in airway segmentation, it is still prone to structural errors, such as missing small bronchi and breaking thin connections. The non-differentiable metrics including BD and TD are not friendly to deep learning models. Both CAS and LSD are implicit loss terms to improve the connectivity measurement since the best supervision signals to characterize the tree-like structure priors are still far away from

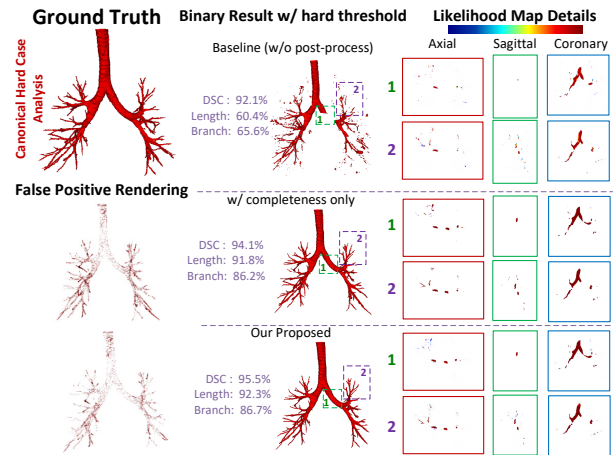


**Fig. 7.** Illustration of binary airway prediction and likelihood maps obtained by different methods. The baseline method generates the skew likelihood map that peripheral airways share lower confidence probability than the principal bronchi, as seen in the likelihood map details of three planes. This problem can be alleviated by the connectivity enhanced methods. Further, false positives are reduced by our proposed approach to maintain the competitive overlap-wise accuracy on top of improving the connectivity.

solved. More specifically, the breakage problem is handled by LSD in this work. However, a generalized representation of segmentation mask is favorable to cover multiple shapes rather than the tree-like structures only.

## C. More Challenges and Future of Airway Segmentation

Both pulmonary disease assessment and endobronchial intervention require accurate airway segmentation for quantitative measurements of bronchial features. Compared with previous works, the proposed method improves the connectivity via balancing the recall/precision metrics and reducing the breakages of small bronchi. This can benefit the accurate counting of airway branches and the navigation to reach the peripheral targets. However, the false positives, as shown in Fig.7, are still not avoidable. As mentioned in [7], the high sensitivity of small bronchi will lead to the over-segmentation of airway which is also not fully addressed in this work. This leads to the higher FPR compared with the best methods. Moreover, the manual annotation can not be perfect due to the existence of complicated airway trees and the limited spacing resolution. These may not be severe issues in the segmentation of large organs while the small changes of ground-truth in the fifth/sixth generations of airway can lead to large variations of local sensitivity of foreground. To overcome this problem, the tree-like structure priors should also consider the confidence of ground-truth labels in the future.

## VI. CONCLUSION

In this paper, we propose a connectivity enhancement network for pulmonary airway segmentation. It contains two critical components, Connectivity-Aware Surrogate Loss (CAS) and Local-Sensitive Distance (LSD) Loss. CAS is designed to simultaneously purses high completeness and high correctness. Furthermore, we introduce the LSD to remove the need for discrete distance operation and construct the corresponding loss function that is perceptible to breakage phenomenon. Experimental results on two public datasets corroborate the proposed method succeeds in preserving the connectivity of airways with competitive voxel-wise/overlap-wise accuracy meanwhile.

## APPENDIX

### A. Proof of Lemma 1

The log-sum-exponential (LSE) is as follows:

$$LSE(d_1, \dots, d_n) = \log(\exp(d_1) + \dots + \exp(d_n))$$

Under the assumption of  $\{d_1 = d_2 = \dots = d_k < d_{k+1} \leq \dots \leq d_n\}$ , the minimum function of  $\beta$ -LSE is defined by:

$$\begin{aligned} \min\{d_1, \dots, d_n\} &= \lim_{\beta \rightarrow -\infty} LSE_\beta(d_1, \dots, d_n) \\ &= \lim_{\beta \rightarrow -\infty} \frac{1}{\beta} \log(\exp(\beta d_1) + \dots + \exp(\beta d_n)) \end{aligned}$$

*Proof:*

$$\begin{aligned} \lim_{\beta \rightarrow -\infty} LSE_\beta(d_1, \dots, d_n) &= \lim_{\beta \rightarrow -\infty} \left[ \frac{1}{\beta} \log(k \exp(\beta d_1) + \sum_{j=k+1}^n \exp(\beta d_j)) \right] \\ &= \lim_{\beta \rightarrow -\infty} \left[ \frac{1}{\beta} \log(k \exp(\beta d_1)) + \frac{1}{\beta} \log\left(1 + \frac{\sum_{j=k+1}^n \exp(\beta d_j)}{k \exp(\beta d_1)}\right) \right] \\ &= \lim_{\beta \rightarrow -\infty} \left[ \frac{1}{\beta} \log(k) + d_1 + \frac{1}{\beta} \log\left(1 + \frac{1}{k} \sum_{j=k+1}^n \exp(\beta(d_j - d_1))\right) \right] \\ &= d_1 \end{aligned}$$

It can be derived that the limitation converges to  $d_1$ , hence the Lemma 1 is proved.  $\blacksquare$

## REFERENCES

- [1] P. Lo, B. Van Ginneken, J. M. Reinhardt, T. Yavarna, P. A. De Jong, B. Irving, C. Fetita, M. Ortner, R. Pinho, J. Sijbers *et al.*, “Extraction of airways from ct (exact’09),” *IEEE TMI*, vol. 31, no. 11, pp. 2093–2107, 2012.
- [2] Y. Qin, M. Chen, H. Zheng, Y. Gu, M. Shen, J. Yang, X. Huang, Y.-M. Zhu, and G.-Z. Yang, “Airwaynet: a voxel-connectivity aware approach for accurate airway segmentation using convolutional neural networks,” in *MICCAI*. Springer, 2019, pp. 212–220.
- [3] A. G.-U. Juarez, H. A. Tiddens, and M. de Bruijne, “Automatic airway segmentation in chest ct using convolutional neural networks,” in *Image analysis for moving organ, breast, and thoracic images*. Springer, 2018, pp. 238–250.
- [4] A. G.-U. Juarez, R. Selvan, Z. Saghir, and M. de Bruijne, “A joint 3d unet-graph neural network-based method for airway segmentation from chest cts,” in *MIML*. Springer, 2019, pp. 583–591.
- [5] D. Jin, Z. Xu, A. P. Harrison, K. George, and D. J. Mollura, “3d convolutional neural networks with graph refinement for airway segmentation using incomplete data labels,” in *MIML*. Springer, 2017, pp. 141–149.
- [6] C. Wang, Y. Hayashi, M. Oda, H. Itoh, T. Kitasaka, A. F. Frangi, and K. Mori, “Tubular structure segmentation using spatial fully connected network with radial distance loss for 3d medical images,” in *MICCAI*. Springer, 2019, pp. 348–356.
- [7] H. Zheng, Y. Qin, Y. Gu, F. Xie, J. Yang, J. Sun, and G.-Z. Yang, “Alleviating class-wise gradient imbalance for pulmonary airway segmentation,” *IEEE TMI*, vol. 40, no. 9, pp. 2452–2462, 2021.
- [8] Y. Qin, H. Zheng, Y. Gu, X. Huang, J. Yang, L. Wang, F. Yao, Y.-M. Zhu, and G.-Z. Yang, “Learning tubule-sensitive cnns for pulmonary airway and artery-vein segmentation in ct,” *IEEE TMI*, vol. 40, no. 6, pp. 1603–1617, 2021.
- [9] T. D. Bui, L. Wang, J. Chen, W. Lin, G. Li, and D. Shen, “Multi-task learning for neonatal brain segmentation using 3d dense-unet with dense attention guided by geodesic distance,” in *DART*. Springer, 2019, pp. 243–251.
- [10] F. Navarro, S. Shit, I. Ezhov, J. Paetzold, A. Gafita, J. C. Peeken, S. E. Combs, and B. H. Menze, “Shape-aware complementary-task learning for multi-organ segmentation,” in *MIML*. Springer, 2019, pp. 620–627.
- [11] X. Hu, F. Li, D. Samaras, and C. Chen, “Topology-preserving deep image segmentation,” *Advances in neural information processing systems*, vol. 32, 2019.
- [12] X. Hu, Y. Wang, L. Fuxin, D. Samaras, and C. Chen, “Topology-aware segmentation using discrete morse theory,” *arXiv preprint arXiv:2103.09992*, 2021.
- [13] S. Shit, J. C. Paetzold, A. Sekuboyina, I. Ezhov, A. Unger, A. Zhylka, J. P. Pluim, U. Bauer, and B. H. Menze, “cldice-a novel topology-preserving loss function for tubular structure segmentation,” in *CVPR*, 2021, pp. 16560–16569.
- [14] E. M. Van Rikxoort, W. Baggerman, and B. Van Ginneken, “Automatic segmentation of the airway tree from thoracic ct scans using a multi-threshold approach,” in *Proc. of Second International Workshop on Pulmonary Image Analysis*. Citeseer, 2009, pp. 341–349.
- [15] S. Born, D. Iwamaru, M. Pfeifle, and D. Bartz, “Three-step segmentation of the lower airways with advanced leakage-control,” in *Proc. of Second International Workshop on Pulmonary Image Analysis*. Citeseer, 2009, pp. 239–249.
- [16] P. Lo, J. Sporring, H. Ashraf, J. J. Pedersen, and M. de Bruijne, “Vessel-guided airway tree segmentation: A voxel classification approach,” *MedIA*, vol. 14, no. 4, pp. 527–538, 2010.
- [17] Y. Qin, H. Zheng, Y. Gu, X. Huang, J. Yang, L. Wang, and Y.-M. Zhu, “Learning bronchiole-sensitive airway segmentation cnns by feature recalibration and attention distillation,” in *MICCAI*. Springer, 2020, pp. 221–231.
- [18] Y. Wu, M. Zhang, W. Yu, H. Zheng, J. Xu, and Y. Gu, “Ltsp: Long-term slice propagation for accurate airway segmentation,” *IPCAI*, 2022.
- [19] Ö. Çiçek, A. Abdulkadir, S. S. Lienkamp, T. Brox, and O. Ronneberger, “3d u-net: learning dense volumetric segmentation from sparse annotation,” in *MICCAI*. Springer, 2016, pp. 424–432.
- [20] S. S. M. Salehi, D. Erdogmus, and A. Gholipour, “Tversky loss function for image segmentation using 3d fully convolutional deep networks,” in *MIML*. Springer, 2017, pp. 379–387.
- [21] P. Krähenbühl and V. Koltun, “Efficient inference in fully connected crfs with gaussian edge potentials,” *NIPS*, vol. 24, pp. 109–117, 2011.
- [22] H. Kervadec, J. Bouchtiba, C. Desrosiers, E. Granger, J. Dolz, and I. B. Ayed, “Boundary loss for highly unbalanced segmentation,” in *MIDL*. PMLR, 2019, pp. 285–296.

[23] Y. Xue, H. Tang, Z. Qiao, G. Gong, Y. Yin, Z. Qian, C. Huang, W. Fan, and X. Huang, “Shape-aware organ segmentation by predicting signed distance maps,” in *AAAI*, vol. 34, no. 07, 2020, pp. 12 565–12 572.

[24] Y. Wang, X. Wei, F. Liu, J. Chen, Y. Zhou, W. Shen, E. K. Fishman, and A. L. Yuille, “Deep distance transform for tubular structure segmentation in ct scans,” in *CVPR*, 2020, pp. 3833–3842.

[25] E. Jang, S. Gu, and B. Poole, “Categorical reparameterization with gumbel-softmax,” *arXiv preprint arXiv:1611.01144*, 2016.

[26] J. D. Cook, “Basic properties of the soft maximum,” 2011.

[27] D. D. Pham, G. Dovletov, and J. Pauli, “A differentiable convolutional distance transform layer for improved image segmentation,” in *GCPR*. Springer, 2020, pp. 432–444.

[28] D. Ulyanov, A. Vedaldi, and V. Lempitsky, “Instance normalization: The missing ingredient for fast stylization,” *arXiv preprint arXiv:1607.08022*, 2016.

[29] K. He, X. Zhang, S. Ren, and J. Sun, “Delving deep into rectifiers: Surpassing human-level performance on imagenet classification,” in *ICCV*, 2015, pp. 1026–1034.

[30] P. Nardelli, K. A. Khan, A. Corvò, N. Moore, M. J. Murphy, M. Twomey, O. J. O’Connor, M. P. Kennedy, R. S. J. Estépar, M. M. Maher *et al.*, “Optimizing parameters of an open-source airway segmentation algorithm using different ct images,” *BEO*, vol. 14, no. 1, pp. 1–24, 2015.

[31] Z. Xu, U. Bagci, B. Foster, A. Mansoor, J. K. Udupa, and D. J. Mollura, “A hybrid method for airway segmentation and automated measurement of bronchial wall thickness on ct,” *MedIA*, vol. 24, no. 1, pp. 1–17, 2015.

[32] E. Smistad, A. C. Elster, and F. Lindseth, “Gpu accelerated segmentation and centerline extraction of tubular structures from medical images,” *IJCARS*, vol. 9, no. 4, pp. 561–575, 2014.

[33] T. Inoue, Y. Kitamura, Y. Li, and W. Ito, “Robust airway extraction based on machine learning and minimum spanning tree,” in *Medical Imaging 2013: Computer-Aided Diagnosis*, vol. 8670. SPIE, 2013, pp. 141–149.

[34] F. Isensee, P. F. Jaeger, S. A. Kohl, J. Petersen, and K. H. Maier-Hein, “nnu-net: a self-configuring method for deep learning-based biomedical image segmentation,” *Nature methods*, vol. 18, no. 2, pp. 203–211, 2021.